Results in Physics 12 (2019) 2189–2201

Contents lists available at ScienceDirect

Results in Physics

journal homepage: www.elsevier.com/locate/rinp

Detailed understanding on the relation of various pH and synthesis reaction times towards a prominent low temperature H_2S gas sensor based on ZnO nanoplatelets

Ioannis Kortidis[a,b], Hendrik C. Swart[c], Suprakas Sinha Ray[a,b], David E. Motaung[a,c,*]

[a] DST/CSIR National Centre for Nanostructured Materials, Council for Scientific and Industrial Research, Pretoria 0001, South Africa
[b] Department of Applied Chemistry, University of Johannesburg, Doornfontein 2028, Johannesburg, South Africa
[c] Department of Physics, University of the Free State, P.O. Box 339, Bloemfontein ZA9300, South Africa

ARTICLE INFO

Keywords:
ZnO nanoplatelets
Point defects
H_2S selectivity
Gas sensing

ABSTRACT

An unceasing scientific challenge to monitor the emissions of toxic and flammable gases in a selective approach is of great importance for safety of human health. As a result, herein, we report on the detailed study of the gas sensing characteristics of ZnO nanostructures prepared at various reaction pH and times. The findings revealed that the variation of synthesis reaction pH and times play a vital role on the morphology and structure. The ZnO-4h@10.5 pH based sensor demonstrated a low response when exposed to reducing gases (CO, CH_4 and NH_3), volatile organic compounds (ethanol, acetone, benzene and toluene) and oxidizing gas (NO_2), while exposed to H_2S gas unpreceded and reproducible response (i.e. 3 times more than the interfering gases) at low operating temperature of 75 °C was observed. The exceptional response (i.e. resistance ratio) observed at the low operating temperature towards 40 ppm H_2S was elucidated by the improved gas accessibility and relative concentration of V_O induced by structural transformation, which induced change in oxygen adsorption. The high H_2S gas selectivity was ascribed to the reactivity of H_2S and low temperature decomposition to participate in a reaction with a ZnO nanoplatelets-based sensor. The fundamental gas-sensing mechanism associated to the ZnO response and point defects at low operating temperature is evaluated in detail.

Introduction

Detection of poisonous and flammable gases for health and security purpose employing semiconductor metal oxides (SMO) based sensors has appealed abundant consideration. This is due to their exceptional advantages, such as a clear evident variation in their sensor resistance when introduced to either reducing or oxidizing gases [1,2], resulting to higher sensitivity, and rapid response-recovery times. Among the n-type SMO, Zinc oxide (ZnO) which is classified as a projecting third-generation has been extensively explored for gas sensing application, because of its good chemical stability, high electron mobility, and non-toxicity [3–5]. While other advantages include synthesis with rich variety of nanostructures and abundant defect properties such as oxygen vacancies (V_O) which behave as shallow donors with changeable hydrogen atoms demonstrating n-type conductivity [6]. The surface V_O can further show a robust adsorption sites for oxidizing molecules. The density of surface V_O hinges on the nature of exposed facet of the SMO [7]. It is well-known that an anticipated gas sensor ought to possess a combination of enhanced sensitivity, excellent selectivity, rapid response-recovery times, long-term stability and low working temperature. These factors are mostly reliant on surface area to volume ratio, higher relative concentration of defects and crystal structure of the SMO sensing layer [8–10]. Kim et al. [11] reported improved sensing response towards ethanol gas, due to higher relative concentration of V_O, possessed by ZnO nanorod array gas sensors. Wang et al. [12] reported the improved ethanol response of the ZnO-300, due to larger amount of the electron donors (V_O and Zn_i), resulting to more adsorbed active oxygen molecules on the ZnO surface. Former reports on ZnO nanorods-based sensor demonstrated that the higher donor defect concentration result to higher sensor response [13–15]. Hosseini et al. [16,17] reported a remarkable response and selectivity to H_2S gas at room temperature using vertically aligned ZnO rods with flower-like structures based sensor and after modification with Au nanoparticles. Ghosh et al. [18] reported an excellent sensing performance using ZnO/γ-Fe_2O_3 heterostructure towards H_2S at an operating temperature of 30 °C. Ramgir et al. [19] reported a room temperature H_2S sensor based

* Corresponding author at: DST/CSIR National Centre for Nanostructured Materials, Council for Scientific and Industrial Research, Pretoria 0001, South Africa.
E-mail addresses: dmotaung@csir.co.za, david.e.motaung@gmail.com (D.E. Motaung).

https://doi.org/10.1016/j.rinp.2019.01.089
Received 12 November 2018; Received in revised form 14 January 2019; Accepted 30 January 2019
Available online 05 February 2019

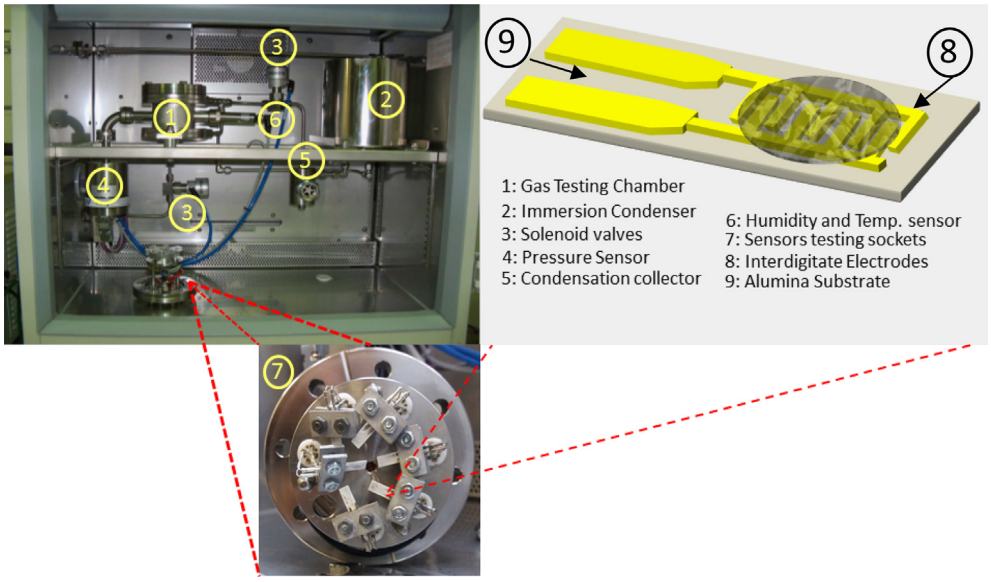

Scheme 1. Schematic diagram of the gas sensing apparatus and the fabricated gas sensing devices used in this work.

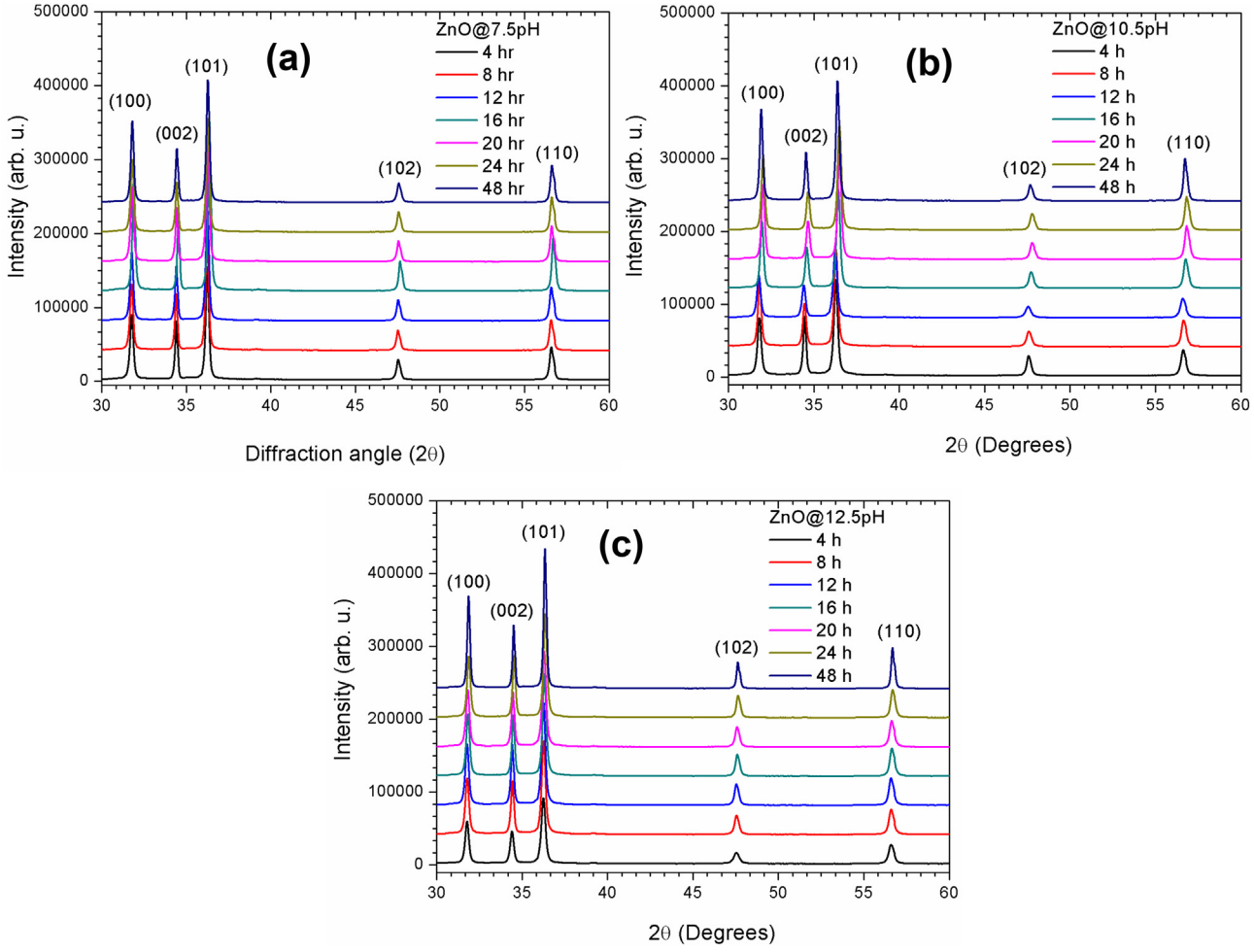

Fig. 1. XRD diffraction patterns of ZnO nanostructures grown at different times and at various pH (a) 7.5, (b) 10.5 and (c) 12.5.

on pure and Au modified ZnO nanowires has been demonstrated. Qi et al. [20] reported that ZnO nanorods decorated with ZnS layer have a superior response to ppm-level of H_2S at room temperature.

Although a significant amount of work exists on detection of H_2S gas using ZnO based sensor, however, only few reports exist at low operating temperatures, since most of the studies are reported at the operating temperatures higher than 100 °C [16–17]. The reports at low operating temperatures are mostly based on ZnO doped with various transitional metals, noble metals and ZnO mixed with combination of other metal oxides [18–21]. Moreover, no detailed study exists

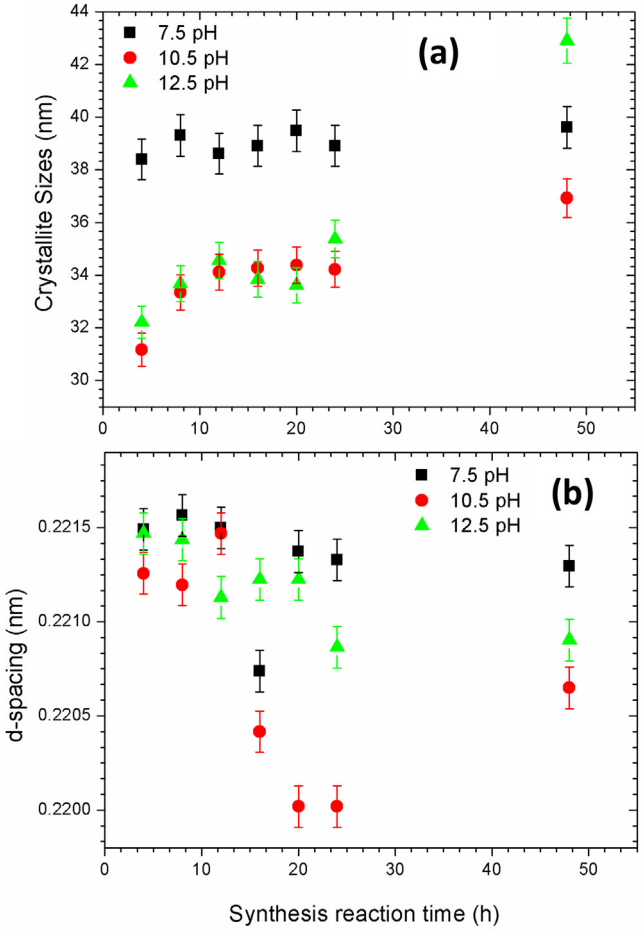

Fig. 2. Evolution of (a) crystallites size and (b) d-spacing of ZnO as a function of synthesis reaction time.

reporting the detection of H_2S using ZnO synthesized at various reaction pH and times (i.e. 4 h to 48 h) to detect H_2S gas at low operating temperature. Our previous study [22] only focused on three reaction times and at 300 °C operating temperature, while the current work focuses on more than six reaction times and showing higher sensitivity at low operating temperature.

Therefore, herein, we combine the ability of synthesizing various ZnO nanostructures at various pH to detect H_2S gas at low operating temperature (75 °C) with higher sensitivity. We demonstrate that the synthesis pH and reaction time play a vibrant role on the morphology, structure and gas sensing characteristics of ZnO nanostructures. The ZnO nanoplatelets prepared for 4 h at 10.5 pH tested to various target gases such as CO, CH_4, NH_3, ethanol, acetone, benzene, toluene and NO_2, exhibited an improved response and remarkable sensitivity to H_2S compared to its counterparts. The effects of relative humidity and long-term stability were also investigated.

Experimental details

Synthesis of various ZnO nanostructures

All chemicals were purchased from Sigma-Aldrich and used as received. Various ZnO nanostructures were synthesized using a facile hydrothermal process. Typically, 0.2 M of $Zn(NO_3)_2{\cdot}6H_2O$ (Zinc Nitrate Hexahydrate) added in 125 mL of deionised water. The pH was adjusted to 7.5, 10.5 and 12.5 by adding 1.0 M NaOH drop wise under vigorous stirring at room temperature. After pH adjustment, the solution was kept under stirring for aging of 2 h. Then, a volume of 125 mL was transferred to a 200 mL volume stainless steel autoclave reactor vessel (Anton Parr) and placed in an oven at 200 °C for 4, 8, 12, 16, 24 and 48 h. The same procedure was carried out for all the samples prepared at various pH. The obtained white solid precipitates were collected by several rinse-centrifugation cycles using deionized water. Then, the products were dried at 90 °C for 12 h and annealed at 200 °C in air for 2 h.

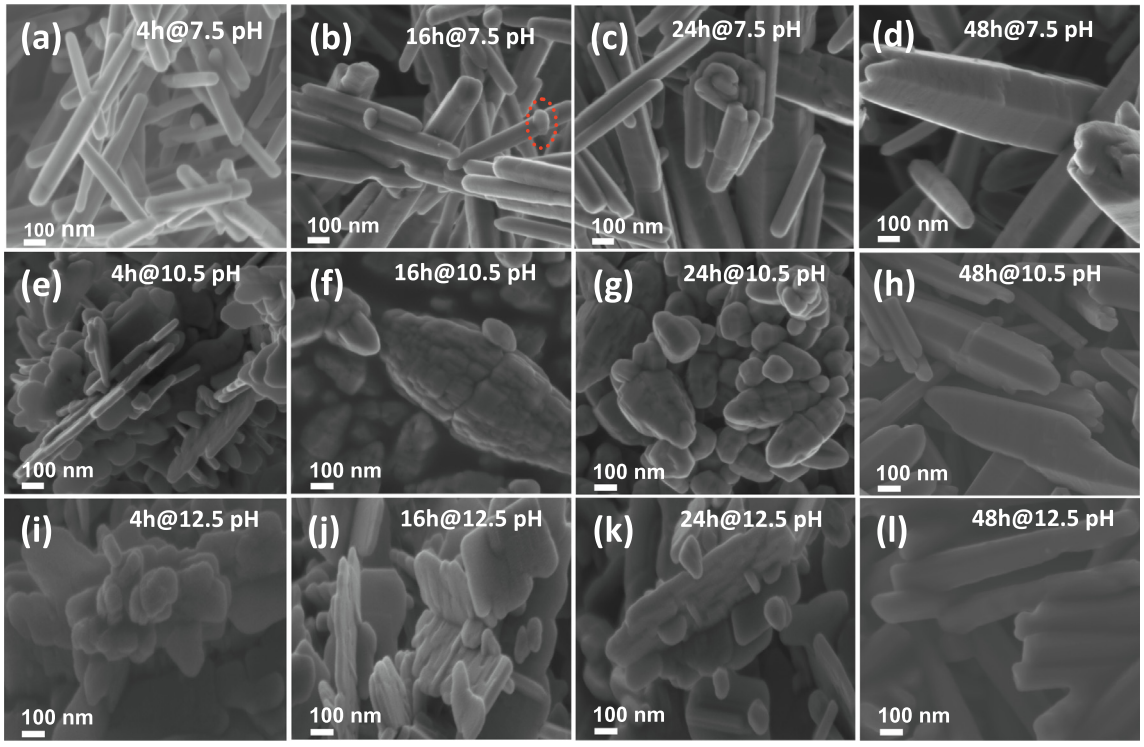

Fig. 3. SEM micrographs of ZnO nanostructures prepared at various pH and synthesis reaction times.

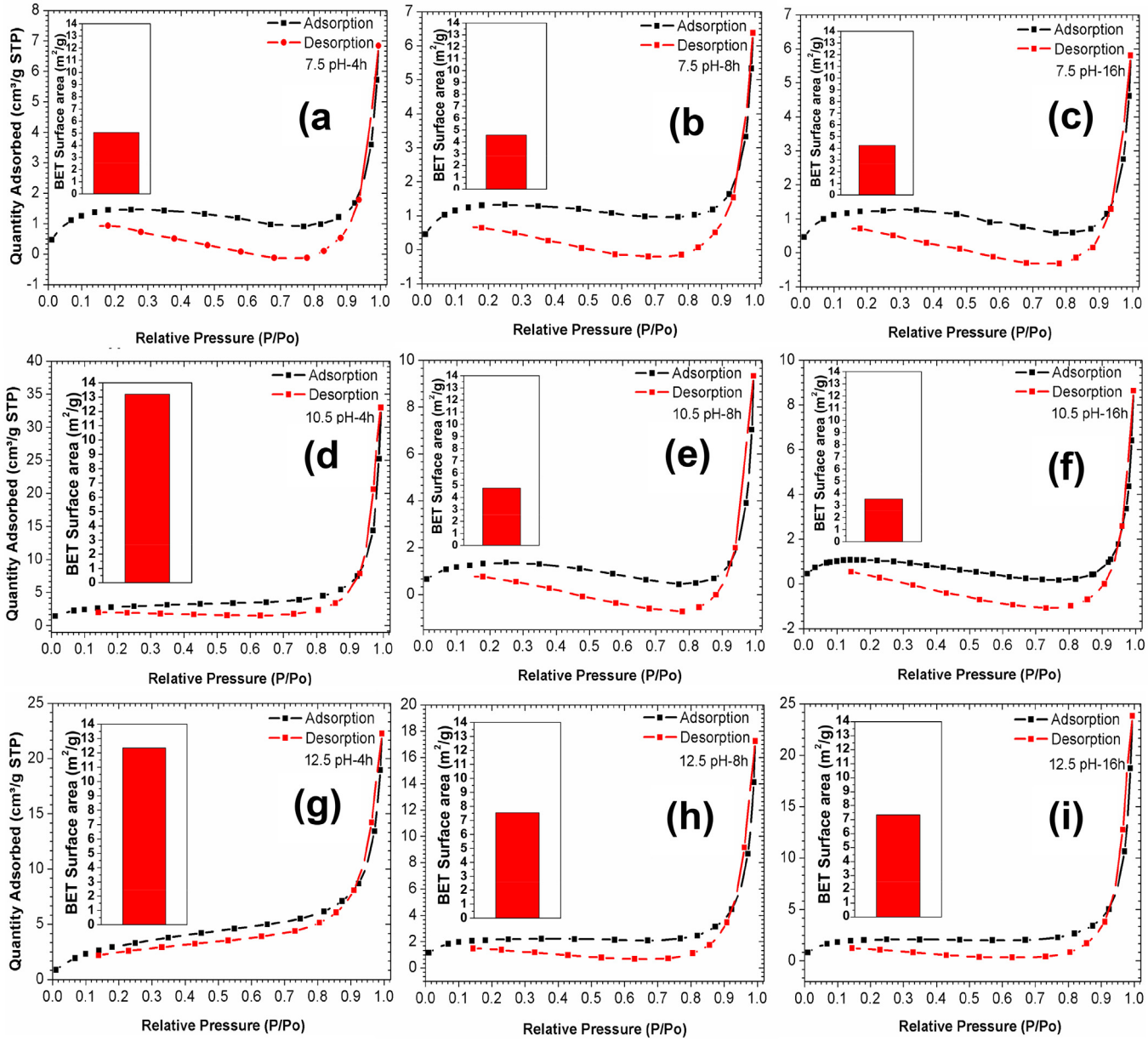

Fig. 4. N_2 adsorption-desorption isotherms of ZnO nanostructures grown at various pH and times (a) 7.5 pH-4 h, (b) 7.5 pH-8h (c), 7.5 pH −16 h, (d) 10.5 pH-4h, (e) 10.5 pH-8h, (f) 10.5 pH-16 h, (g) 12.5 pH-4h, (h) 12.5 pH-8h and (i) 12.5 pH-16 h. Insets correspond to S_{BET}.

Characterization

X-ray powder diffraction (XRD) patterns of various ZnO nanostructures were examined using a Panalytical X' pert Pro PW 3040/60 (Netherlands). The surface morphology was investigated using a Zeiss scanning electron microscopy (SEM). The N_2 adsorption-desorption isotherms and Brunauer, Emmett and Teller (BET) surface area were characterized by Micromeritics TRISTAR 3000 (USA). The photoluminescence (PL, France) measurements were analyzed using a Horiba Jobin-Yvon NanoLog spectrometer at an excitation wavelength of 330 nm. A PHI 5000 Versaprobe-Scanning ESCA Microprobe instrument (ESCA, USA), X-ray photoelectron spectroscopy (XPS), was used to study the chemical composition of various ZnO nanostructures.

Fabrication and characterization of ZnO gas sensors

The gas sensing measurements were carried out by placing an appropriate amount of ZnO sample powder in an agate mortar and grounded by adding a terpineol to form a slurry, then drop-coated onto the alumina substrates pre-printed with a platinum electrode on the top surface and a resistive micro-heater on the bottom surface. Then, the dried sensing films at 100 °C for 3 h were inserted into an airtight test chamber (see Scheme 1) at a controlled temperature, under different conditions (i.e. in dry air and under relative humidity of 40–60%). The fabricated ZnO sensors were exposed to different concentrations (5–100 ppm) of various reducing gases (CO, CH_4 and NH_3), volatile organic compounds (ethanol (C_2H_5OH) and acetone (C_3H_6O), benzene (C_6H_6) and toluene (C_7H_8)), as well as an oxidizing gas (NO_2). The measurements were carried out at various operating temperatures ranging from room temperature (23 °C) to 175 °C. The electrical resistance of the ZnO sensing devices to various gas concentrations was measured using a KSGAS6S gas testing station (KENOSISTEC, Italy).

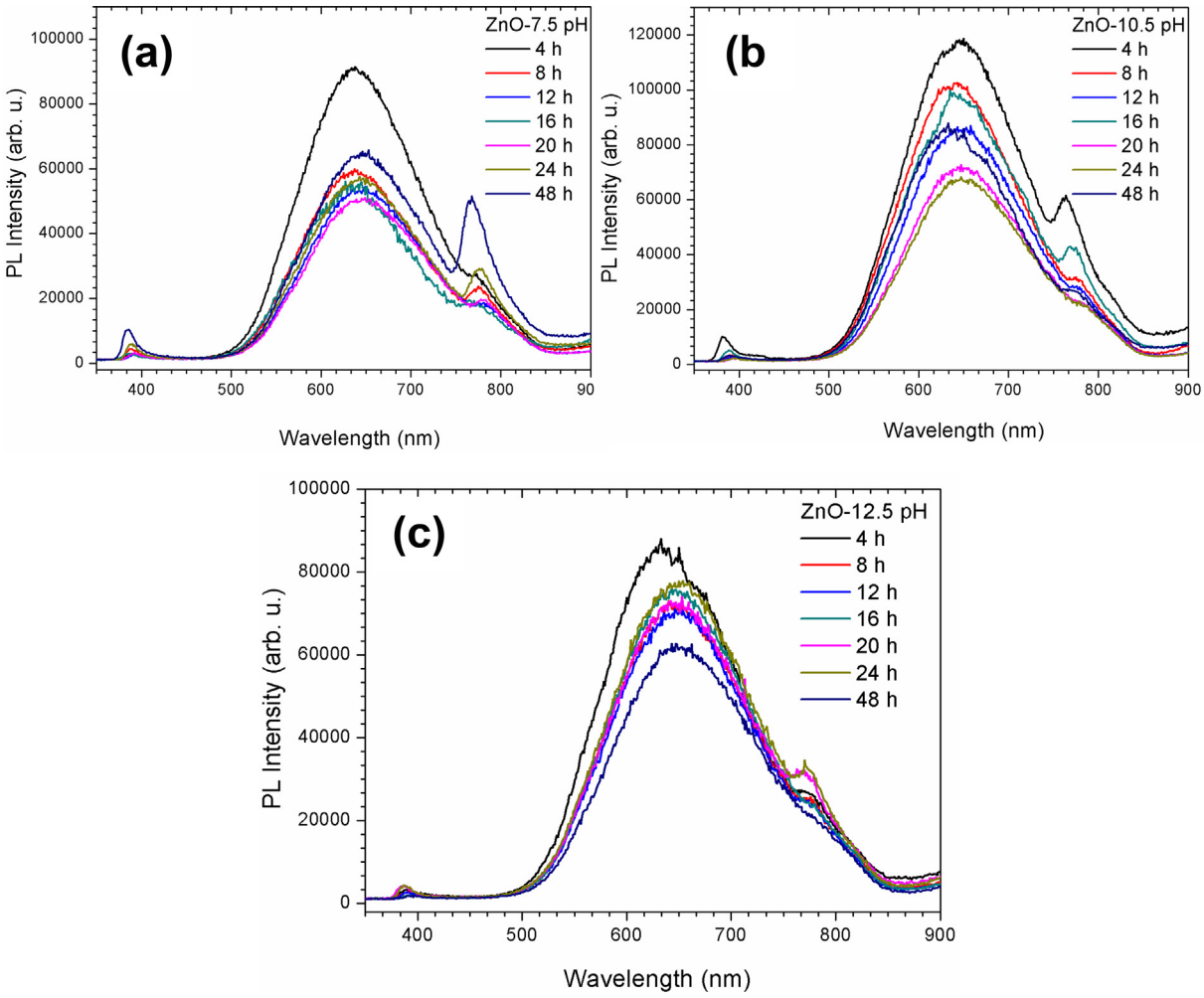

Fig. 5. Room temperature PL spectra of various ZnO nanostructures grown at different pH and synthesis reaction times (a) 7.5, (b) 10.5 and (c) 12.5.

Results and discussions

Structure and morphology

XRD patterns of various ZnO-nanostructures grown at different pH and times are exhibited in Fig. 1. Based on the XRD patterns, all the peaks could be indexed to the standard wurtzite ZnO (JCPDS No. 36-1451). No other additional peaks were detected, which validate that the as-prepared ZnO nanostructures were of high quality. From all the structures grown at different pH, a size-dependent broadening due to the increase in the reaction temperature is observed. Oosthuizen et al. [23] reported a similar behaviour on the CuO nanoplatelets grown at different reaction temperatures. The estimated average crystallite sizes of the prepared various ZnO nanostructures using Scherrer formula [24] are shown in Fig. 2. As presented in Fig. 2, the crystallite sizes increase, with an increase in synthesis reaction time. A peak shift is observed (see Supplementary electronic information (ESI), Fig. S1) and this is validated by the shifting of the d-spacing, (see Fig. 2b) as the synthesis reaction time increases.

The SEM micrographs of the ZnO nanostructures prepared at various pH and times are displayed in Fig. 3. In Fig. 3a, the nanorods grown for 4 h at a 7.5 pH are smooth. And their diameter is in the range of 80–100 nm. In a weak basic solution such as 7.5 pH, $Zn(OH)_2$ solid precipitate exists in the reactant solution, due to the rapid growth rate along the [0002] direction than along the other directions. The ZnO nuclei grow into nanorods in the same [0002] direction [25,26]. At longer synthesis reaction time, 16 h, the nanoparticle are dispersed on the edges of the nanorods (see red circle). At the synthesis reaction time of 24 h, the size of the nanorods increases, showing a hexagonal shape morphology, which is clearer on the image of the 48 h sample (see Fig. 3d). The pores observed on the edges of the rods at 48 h, are probably due to the etching induced by the long synthesis reaction time. At a pH of 10.5, nanoplatelet-like structures with a diameter of approximately 30 nm are observed. In a more basic condition, all dissolved $Zn(OH)_2$ forms a complex $Zn(OH)_4^{2-}$ growth units, which have a negative charge. Moreover, a significant quantity of nucleophilic OH^- remains in the solution and can easily be adsorbed on to the positive polar surfaces. As a result, $Zn(OH)_4^{2-}$ complex finds it difficult to be incorporated on the positive and negative surface of ZnO. This hinders the crystal growth along (0001) direction and results in nanoplatelets like morphology [26]. Increasing the synthesis reaction times to 16–24 h, the cone-like structures are observed, which become smoother at 24 h. While at 48 h (see Fig. 3h), the shape transforms to nanorods which appear to be broken.

When increasing the pH to 12.5 pH at the synthesis reaction time of 4 h, large particles are observed, which further self-assembled to platelets with diameter of approximately 45–50 nm (i.e. larger than that seen for 7.5 pH at 4 h) at 16 h synthesis reaction time. At a higher pH value of 12.5, the reaction occurs at a rapid rate providing a nucleation dominated process, leading to the formation of nanoparticles which self-assemble to the formation of nanoplatelets in an arrangement of flower-like structure having no preferred orientation. At 24 h, the diameter of the platelets increases and smaller particles attached to the platelets side are also observed. At the synthesis reaction time of 48 h,

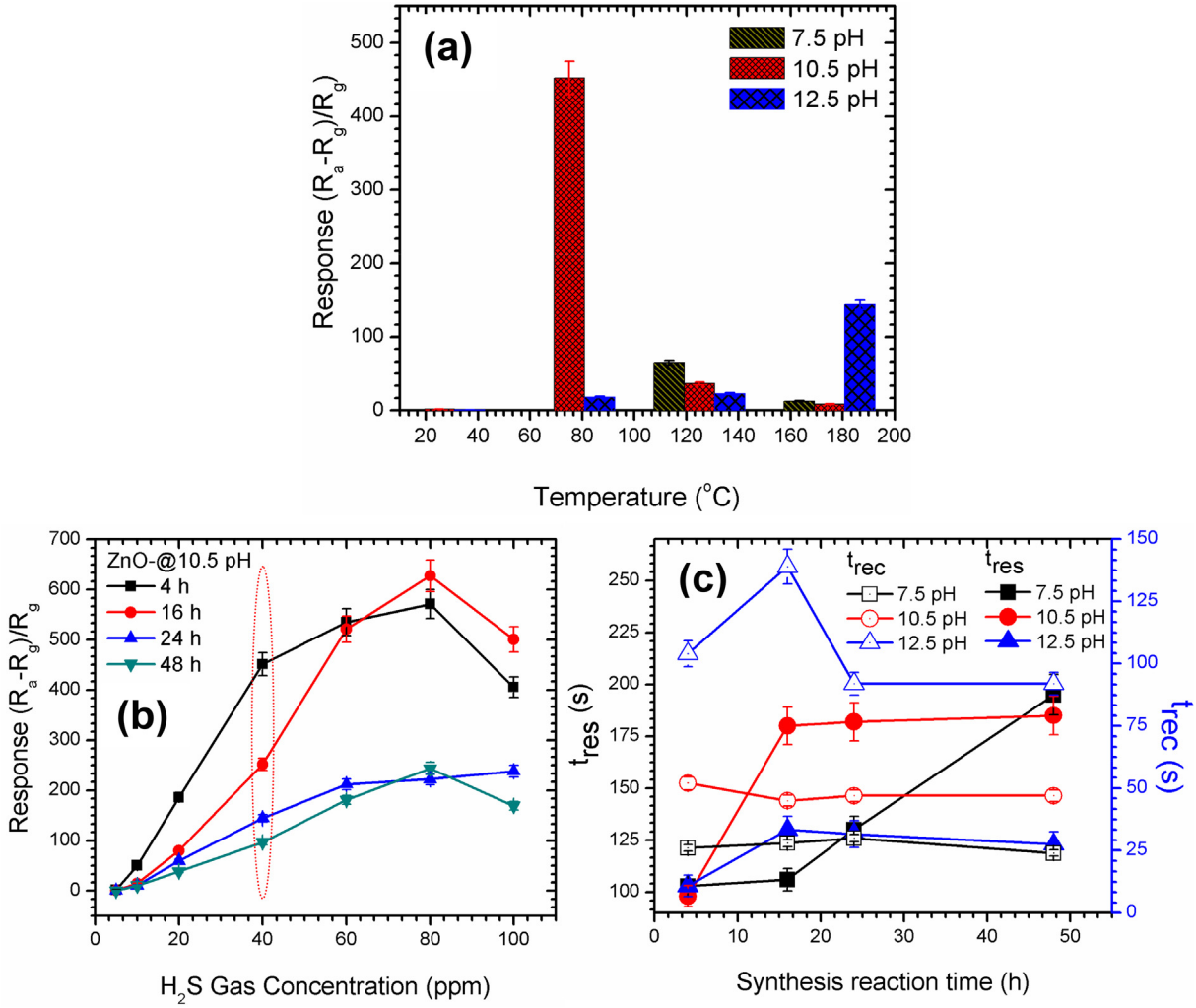

Fig. 6. (a) Response versus temperature for the ZnO at 40 ppm H_2S (Note: 10.5 and 12.5 pH samples were prepared for 4 h and that of 7.5 pH was prepared for 24 h, since they showed best response), (b) response versus gas concentration for ZnO@10.5pH, and (c) response-recovery times plot versus synthesis reaction time of ZnO towards H_2S gas (Note: all the sensor data was extracted at 75 °C).

Fig. 3l, rod-like structures are observed attached to one another.

Brunnauer–Emmett–Teller surface analysis

The textural properties of ZnO nanostructures were explored by N_2 adsorption/desorption analyses as demonstrated in Fig. 4. The samples led to typical type III with pore diameter in the range of 4–100 nm varying the synthesis pH. Besides, the higher BET surface areas (S_{BET}) of 13.2035 and 12.3454 m^2/g are observed for samples prepared for 4 h at 10.5 and 12.5 pH (see Fig. 4), respectively. In Fig. S2 the pore diameter of the 7.5 pH decreases with the synthesis reaction time; while that of the 10.5 pH increases from 4 h to 24 h, then decreases at 48 h reaction time. At 12.5 pH, the pore diameter increases with the synthesis reaction time. It is further evident that the reaction pH and the time affect the structure of the materials as confirmed from the SEM and XRD analyses, showing that the morphology and texture of the materials transformed, while the crystallite sizes increased with an increase in synthesis reaction pH and time. Previous studies have shown that higher S_{BET} is very beneficial for gas sensing performance [27].

Previous studies have reported that point defects such as oxygen vacancies (V_O) in ZnO influence the surface chemistry and electronic properties of the sensing material [28,29]. Fig. 5 shows distinctive room temperature PL spectra of the ZnO nanostructures. All the spectra show a small PL emission at 375–380 nm related to near band edge (NBE) emission [28,30]. At higher wavelengths (500–850 nm) a strong broad PL emission covering the blue-green (~480–550 nm), yellow (~550–600 nm), and orange-red (~600–850 nm) regions [30] is observed. The peak intensities decrease with an increase in synthesis reaction time. By deconvoluting the spectra in the range of 500–850 nm using Gaussian fit, six peaks are observed (see ESI, Fig. S3). According to the literature, a peak positioned at 548 nm is associated to oxygen vacancies (V_O), while the emission around 585 nm is associated to the doubly ionized oxygen vacancy [31–34]. The PL emission in the range of 625–650 nm is related to oxygen interstitials (O_i) [35]. Previous studies have reported that the near-IR emission at 750–800 nm is related with oxygen-related defects [29]. While a report by Gomi et al. [36] suggested that interstitial zinc may be the reason for the red and IR emission in ZnO. Besides, by comparing all the spectra, the ZnO-4h@10.5pH shows a higher green emission relative to UV emission, signifying substantial defects related to V_O. These findings are also confirmed by electron paramagnetic resonance analyses shown in the ESI, Fig. S4. Whereby a paramagnetic signal at g-factor of 1.99 related to V_O [37,38] was higher for the ZnO-4h @10.5 pH compared to its counterparts. We further observed higher number of spins for ZnO-4h@10.5pH (Table S1 and Fig. S5a). Therefore, this confirm the estimated value of the relative intensity of the visible emission and ultraviolet (Vis/UV), extracted from the PL spectra is approximately 12.69 for the ZnO-4h@10.5pH compared to its counterparts. Previous studies have

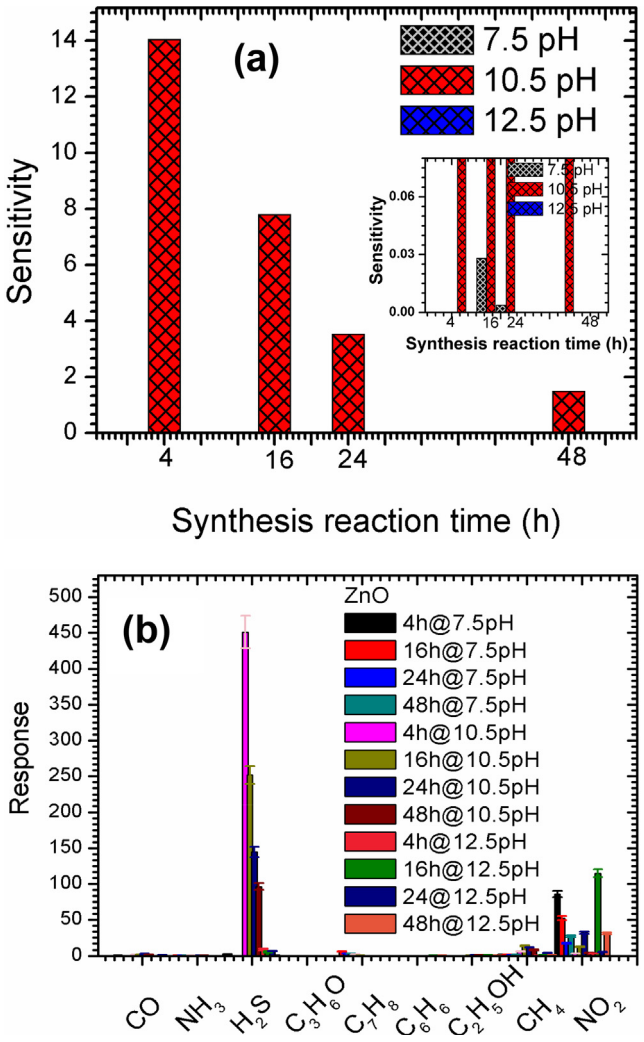

Fig. 7. (a) Sensitivity of various ZnO towards H_2S at 75 °C and (b) selectivity plot of various ZnO nanostructures tested towards 40 ppm of different gases at 75 °C.

reported that a higher relative concentration of V_O improves the sensor response via enhanced adsorptions of oxygen molecules increasing the interrelation with target gas molecules [23,29,31].

Electrical and gas-sensing characterization

The temperature-dependence of the sensors responses was studied in dry air in the temperature range of 23–175 °C at 40 ppm H_2S gas as shown in Fig. 6. Generally, the sensor response is defined as $(R_g - R_a)/R_a$ and $(R_a - R_g)/R_g$ in oxidizing and reducing gases, respectively, where R_a and R_g are the resistance of the sensor in air and target gas, respectively [39]. As presented in Fig. 6, the higher response of approximately 451 is observed at 75 °C. Further increase in the operating temperature, decreases the response. This clearly shows that H_2S can be decomposed at lower operating temperature by forming ZnS (see XPS section) resulting to improved sensing response [40,41]. More remarkably, it is clear that from all the sensing materials, only the ZnO-4h@10.5pH displays improved response compared to its counterparts. Based on the PL and BET studies, this sensing material revealed higher point defects and surface area, justifying the observed remarkable response. The drop in response for ZnO@10.5pH is because of the adsorption saturation, when the operating temperature elevates, the H_2S gas is desorbed before it interacts with the oxygen ions on the ZnO surface, therefore reducing the response [27]. Nonetheless, for the ZnO@12.5pH the response increases with an operating temperature, showing a higher response at 175 °C, suggesting that the activation of H_2S reaction with adsorbed oxygen molecules on the ZnO@12.5pH surface need considerably higher operating temperatures.

In addition, the sensing response versus H_2S gas concentration (i.e. 5–100 ppm) was studied as displayed in Fig. 7b. The responses of the ZnO sensing layers grown at various reaction times (i.e. 10.5 pH) increase with H_2S gas concentration. While that grown for 4 h saturates at 40 ppm (see a circle), denoting that it is only stable up to 40 ppm. A clear decrease in responses is observed at 80 ppm.

To monitor the operation of a gas sensor in the real-time environment, a sensor exhibiting a rapid response (t_{res}) and recovery (t_{rec}) times is compulsory. The t_{res} and t_{rec} of gas sensor are defined as the time needed to achieve 90% of the absolute resistance when exposed to a target gas and above 10% of its original value once the target gas is removed, respectively [42]. The t_{res} and t_{rec} curves of the ZnO as a function of reaction times for samples grown at various pH exposed to 40 ppm of H_2S are shown in Fig. 6c. As shown in Fig. 6c, the shorter t_{res}

Table 1
Comparison of H_2S gas sensing performances based on ZnO.

Sensing layer	Gas Concen. (ppm)	Operating Temp. (°C)	Response	$\tau_{res.}$ (s)	$\tau_{rec.}$ (s)	Refs.
ZnO nanoplatelets	**40**	**75**	**451**	**93**	**51**	**Current work**
ZnO:Au aligned nonorods films	3	25	~450	660	720	Hosseini et al. [17]
ZnO:Au nanowires	5	25	79	~450	170	Ramgir et al. [19]
ZnO:Ni films	100	25	321	12	90	Mani et al. [21]
ZnO/γ-Fe_2O_3	10 000	30	82	~300	~600	Ghosh et al. [18]
ZnO-CuO nanotetrapod films	10	50	3.5	–	~1000	Kaur et al. [49]
ZnO Quantum dots films	68.5	90	575	~550	~500	Deng et al. [50]
ZnO-CuO mesocrystals	10	125	152	180	356	Guo et al. [51]
ZnO honeycomb-like	50	135	65.6	51	179	Meng et al. [52]
ZnO nanowires film	2	150	0.9	180	60	Huang et al. [53]
ZnO-CuO nanofibers	10	150	4490	–	–	Katoch et al. [54]
ZnO nanorods	100	190	97	5	16	Cao et al. [55]
ZnO:Ti films	20	200	0.29	~12	~125	Shewale et al. [56]
ZnO microspheres	0.5	220	51	219	227	Diao et al. [42]
ZnO:Cu films	20	250	38	~17	~12	Shewale et al. [57]
ZnO nanorods	60	300	8385	~77	~76	Motaung et al. [22]
ZnO:Mo nanowire	5	300	14.1	~150	~50	Woo et. al. [58]
ZnO:Pd nanorods	500	300	~1900	720	36,000	Hieuet. al. [59]
ZnO tetrapods films	1	350	~30	~150	~240	Calestani et al. [45]
ZnO films	12	450	1.8	~20	–	Ghimbeau et al. [60]
ZnO nanorods	50	500	35	~1080	~300	Kim et al. [61]

The boldness refers to the current work in order to compare with the literature.

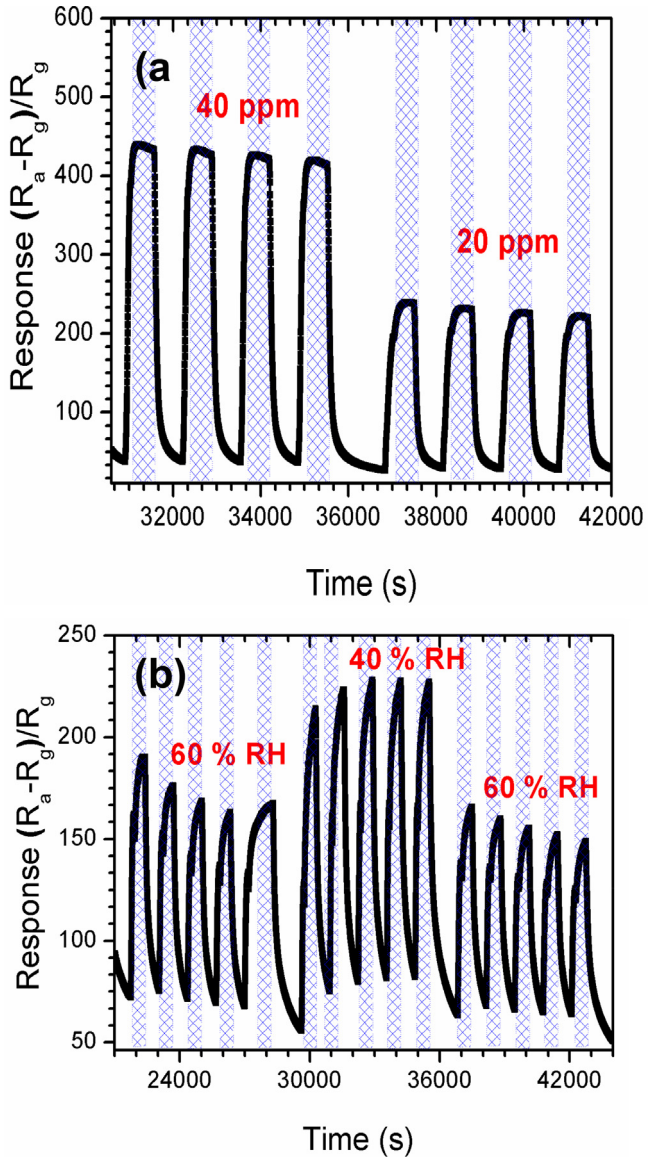

Fig. 8. Repeatability measurements of ZnO-4h@10.5pH towards various H_2S concentrations, and (b) real-time response towards 40 ppm H_2S in the presence of various RH (40 and 60%).

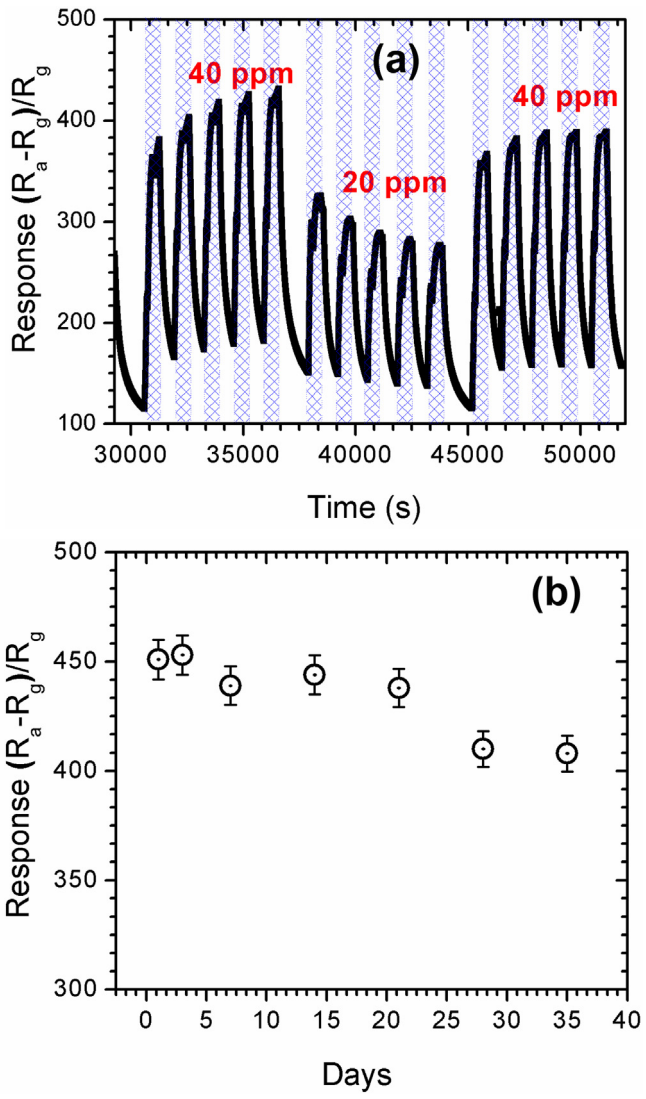

Fig. 9. Long-term stability plot in a real time-response towards 20 and 40 ppm H_2S gas and (b) Stability plot in terms of days.

of approximately 97 s is documented for the 10.5 pH sensing material prepared for 4 h.

To evaluate the sensitivity of the ZnO based sensors towards H_2S gas, we used the slope of the plots shown in Figs. 6 and S3b, ESI [27]. The sensitivity analyses were extracted at the temperature of 75 °C. The ZnO-4h@10.5pH shows a higher sensitivity (value of 14.04 ppm^{-1}) compared to its counter parts showing less selectivity, as shown in the inset of Fig. 7a. Moreover, it is observed that the sensitivity values decrease with an increase in synthesis reaction time. This improved gas sensitivity observed for the ZnO-4h@10.5pH gas sensor is due to smaller crystallite size, higher pore diameter and point defects. According to the reports by Rout et al. [43] and Chen et al. [44] pore diameter of the nanostructures has a considerable influence on the sensitivity performance of the sensor.

Gas selectivity is precisely imperative for real-world application. Generally, H_2S is considered as a toxic, corrosive and combustible gas and it is typically found in natural gas industries, crude petroleum, etc. Consequently, real-time detection and monitoring in the low concentration is the utmost vital for the human health safety [45,46]. Therefore, the selectivity plot of ZnO nanostructures to various reducing gases (CO, CH_4, H_2S, and VOCs like benzene, toluene and acetone) and oxidizing gas (NO_2) towards 40 ppm at 75 is presented in Fig. 7b. As demonstrated in the selectivity plot (Fig. 7b), the ZnO-4h@10.5pH tested at 75 °C have the highest response value of 451 at 40 ppm, followed by 16 h and 24 h with response values of 251 and 145, respectively. This excellent selectivity of the sensor can be ascribed to extraordinary reactivity of H_2S and low temperature decomposition of H_2S to participate in reaction with sensing material [41,46]. ZnO possess greater affinity to H_2S gas with relation to other tested gases [41]. Thus, the significant difference in sensors response values suggests that the ZnO-4 h @10.5pH sensor has a sustaining selective ability to H_2S contrary to other tested gases.

For quantification, the selectivity values were computed using the following relation, $S = S_a/S_b$, where S_a and S_b are the responses of a sensor towards target gas and interfering gas, respectively [47,48]. Therefore, from the calculated selectivity values of S_{H2S}/S_{CO}, S_{H2S}/S_{NH3} S_{H2S}/S_{C3H6O}, S_{H2S}/S_{C6H6}, S_{H2S}/S_{C7H8}, S_{H2S}/S_{NH3} and S_{H2S}/S_{C2H5OH}, S_{H2S}/S_{C2H5OH} and S_{H2S}/S_{NO2}, the ZnO-4h@10.5pH sensor revealed the highest value of approximately 7516 for the H_2S over the interference gas C_2H_5OH, while the 16h@10.5pH based sensor disclosed a value of approximately 6295 for the H_2S over the interference gas of C_3H_6O. The improved sensitivity to H_2S gas and exceptional selectivity in the presence of various interfering gases signifies the practice of ZnO-4h@

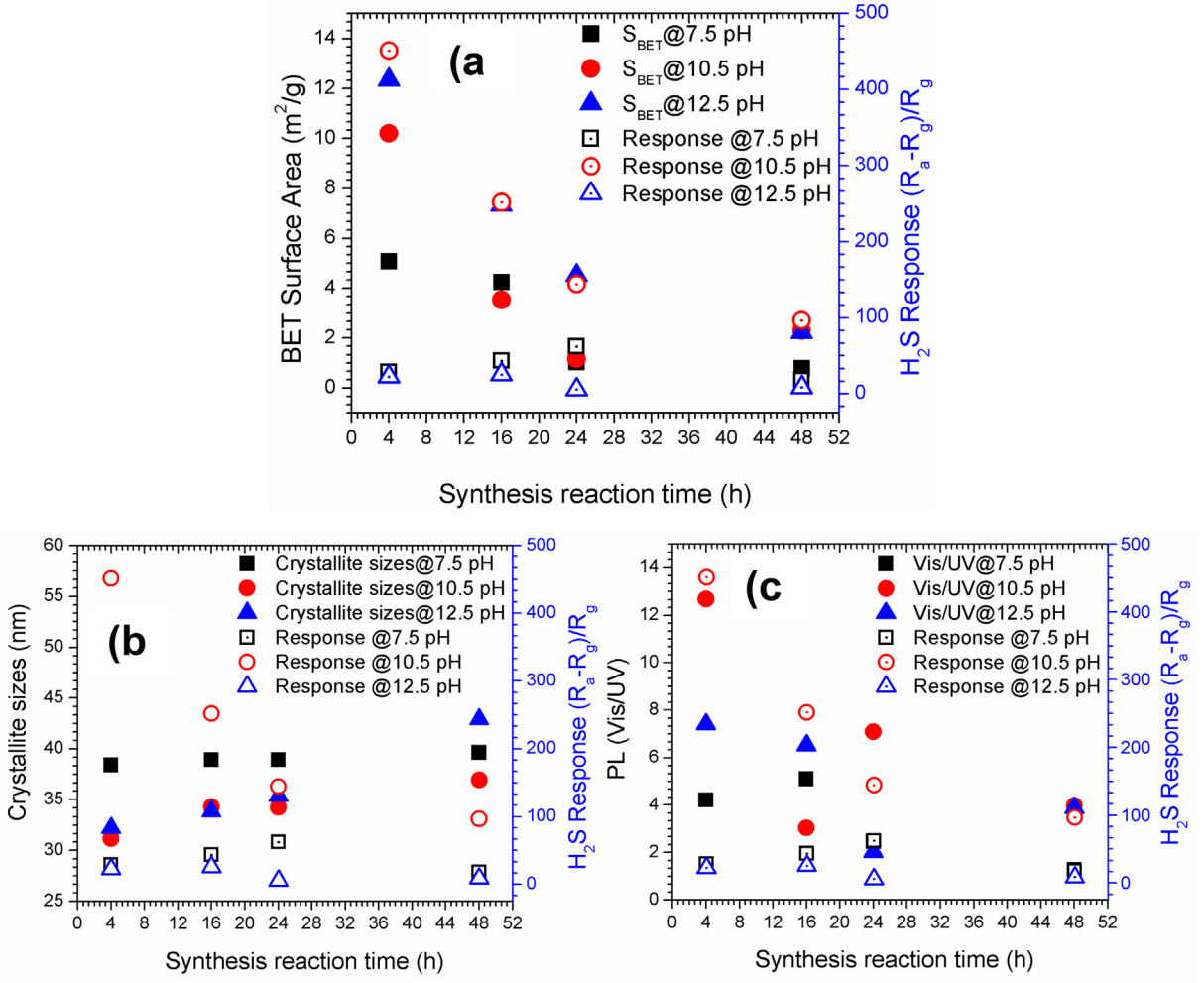

Fig. 10. Response of various ZnO nanostructures versus (a) BET surface area, (b) crystallite sizes and (c) PL (Vis/UV) ratio related to point defects.

10.5pH based sensor for detection and monitoring of H_2S gas in practical application.

The H_2S gas sensing ability of ZnO nanoplatelets prepared in this work for 4h@10.5 pH is compared with the commercially available H_2S sensor, which is showing a response of 82 at 10,000 ppm and operating temperature of 30 °C [18]. Our work is also compared with other 20 various gas sensors fabricated from pure and doped ZnO nanostructures such as ZnO:Au nanowires, ZnO:Au aligned nonorods films, ZnO:Ni films, ZnO-CuO nanotetrapod films, ZnO-CuO mesocrystals, ZnO:Mo nanowire, etc. As listed in Table 1, this comparison is done for the ZnO-based sensors measured at various operating temperatures (i.e. 25–500 °C) and gas concentrations (1–10,000 ppm). Therefore, the current H_2S gas sensor in association to the commercially available SMO based sensor and that listed in Table 1 as well as that published in our previous work shows a comparable response at low operating temperature and low gas concentration. More remarkably, most of the sensors shown in the literature are doped or incorporated with transitional or noble metals still display a low response compared to our findings.

In addition to the sensitivity and selectivity, the sensor reproducibility and stability are vital performance indicators and as well as critical parameters for real-time application. Fig. 8a illustrates the reproducibility plot of the ZnO nanoplatelets-based sensor, which was consecutively tested towards 20 and 40 ppm H_2S gas for four successive cycles at 75 °C. It is apparent that the repeated adsorption-desorption of H_2S gas for four times are virtually indistinguishable, disclosing a clear firm response ability curves with a maximum response of about 445–at 40 ppm of H_2S. This reveals a fair reversibility and repeatability behaviour of the ZnO sensor at all levels of the H_2S gas concentrations.

For a gas sensor functioning at a low temperature such as 75 °C, the response of sensing material is generally established not to be stable under the relative humidity (RH) [62,63]. Fig. 8b shows the sensor response of ZnO-4h@10.5pH tested towards 40 ppm H_2S for five successive cycles in the presence of various RH levels of 40 and 60% at 75 °C. As shown in Fig. 8b, although the initial response value reduced by 49% in the presence of 60% RH compared to the original value of 451 in dry air, however, it is clear that our sensor is very stable to RH after being exposed to 40 ppm H_2S for five successive cycles in the presence of 40 or 60% RH. Previous studies have reported that the gas sensing response decreases with an increase in relative humidity in the range of 20–60% [64–65].

To further validate the stability of the sensor, the long-term stability was carried out by placing the gas sensor in a room ambient condition for about 3 weeks and re-used to test towards different H_2S concentrations (20 and 40 ppm) for four cycles at 75 °C. As a result, the plot displayed in Fig. 9a demonstrates a comparable response behaviour compared with that in Fig. 8a (i.e. fresh sensor) after 3 weeks. Fig. 9b shows a stability plot in terms of days. As shown in Fig. 9b, the sensor response is stable for 21 days. However, after 35 days of exposure to H2S, a response dropped by 9.53%. These findings prove that our sensor has a fair stability and pleases the necessary requirements for H_2S gas detection in practice.

To verify the sensing results further, extensive investigation was carried out by associating our sensing response with the BET surface

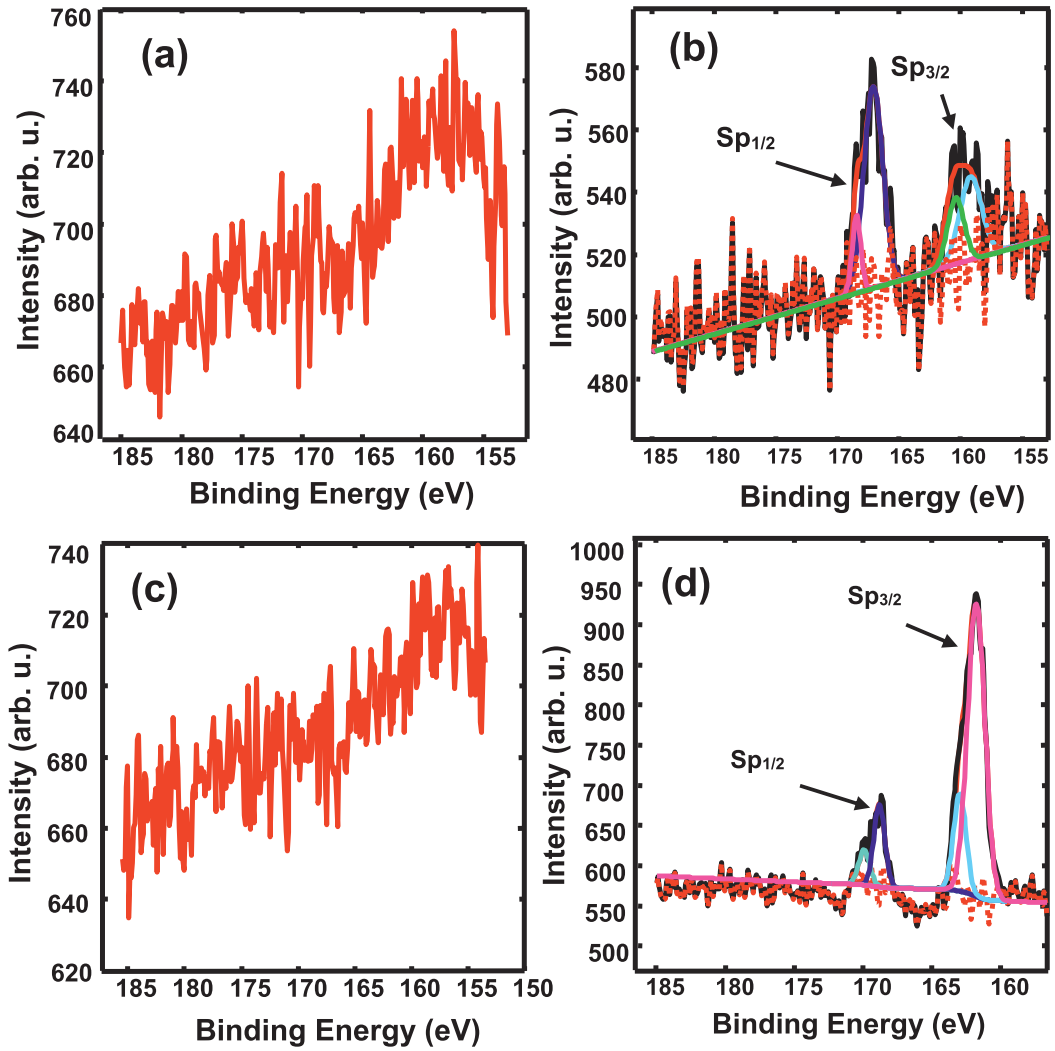

Fig. 11. S2p XPS spectra of (a and b) ZnO-4h@10.5pH and (c-d) ZnO-4h@12.5pH sensing layers before and after exposure to H_2S gas.

(S_{BET}), crystallite sizes and the relative intensity of the visible emission and ultraviolet (Vis/UV) extracted from the PL spectra as a function of synthesis reaction pH and time, as shown in Fig. 10. It is observed in Fig. 10a that from all the samples, the 10.5 pH sample prepared for 4 h has the highest sensing response of 451 and S_{BET} of 13.2 m^2/g. However, as the S_{BET} decreases with the synthesis reaction time, the sensing ability also decreases and this behaviour is also noted for the samples prepared at 7.5 and 125 pH. Oosthuizen et al. [23] also observed that as the S_{BET} decreases with the synthesis reaction temperature, the response of the CuO nanoplatelets based sensor also decreases.

As demonstrated in Fig. 10b, the sensing response towards 40 ppm H_2S increases when the average crystallite sizes decreases, especially for the sample grown for 4 h at 10.5 pH. However, as the crystallite sizes increases due an increase in synthesis reaction time, the sensing ability reduces. This clearly justifies that sensing ability of the nanostructures is reliant on the V_O, because the V_O are the utmost considered adsorption sites for oxygen species resulting to enhanced interrelation with the target gas molecules, as confirmed in see Fig. 10c, showing a clear decrease in response with the relative PL ratio of the Vis/UV plot [23]. This basically shows that the crystal quality of the nanostructures increased, as validated by the XRD findings. This behaviour is also observed for the samples prepared at the pH of 7.5 and 12.5.

To confirm the influence of sulfuration behaviour on the ZnO-4h@10.5pH and ZnO-4h@12.5pH sensing layers surface exposed to H_2S gas at 75 and 125 °C, respectively, XPS studies were extracted and results are presented in Fig. 11, while the survey spectra are shown in ESI, Fig. S5. The binding energies were calibrated with respect to the carbon peak identified around 285.0 eV. In Fig. 11a and c, both ZnO-sensing layers do not display any S_{2p} peaks before exposure to H_2S gas. The S_{2p} peaks of the ZnO-4h@10.5pH sensing layer (Fig. 11b) exposed to H_2S gas are positioned at 167.1 and 168.4 eV linked to $ZnSO_4$ [66,67] and S^{2-} from ZnS nanostructure at 161.0 and 160.0 eV. The ZnO-4h@12.5pH sensing layer exposed to H_2S also displays the two core S_{2p} peaks deconvoluted into 169.9, 168.3 eV and 161.8 and 163.0 eV, validating the formation of $ZnSO_4$.

The O1s spectra of ZnO-4h@10.5pH and ZnO-4h@12.5pH in Fig. 12a and c present a broad peak fitted into three peaks centred at around 529.0, 530.1 and 531.8 eV and 529.0, 530.3, 531.8 eV before H_2S exposure, respectively. The peaks centred at 529.0, 530.1, 531.8 eV and 532.2 eV are related to O^{2-} ions in the wurtzite structure, O^{-2} ions in the oxygen deficient regions, linked to V_O, and presence of unattached bound oxygen on the ZnO surface, respectively [66,67]. It is clear that the ZnO-4h@10.5pH shows more ratio of V_O, which is minimal for the ZnO-4h@12.5pH (see Table S1), validating the PL analyses. Upon H_2S exposure, additional O1s peak at 531.9 eV related to $ZnSO_4$ is observed for both ZnO-4h@10.5pH and ZnO-4h@12.5pH, respectively. This observation confirms the formation of $ZnSO_4$ and this is also witnessed by the shifting of both O1s and Zn2p peaks to higher binding energy after H_2S exposure (see ESI, Fig. S6).

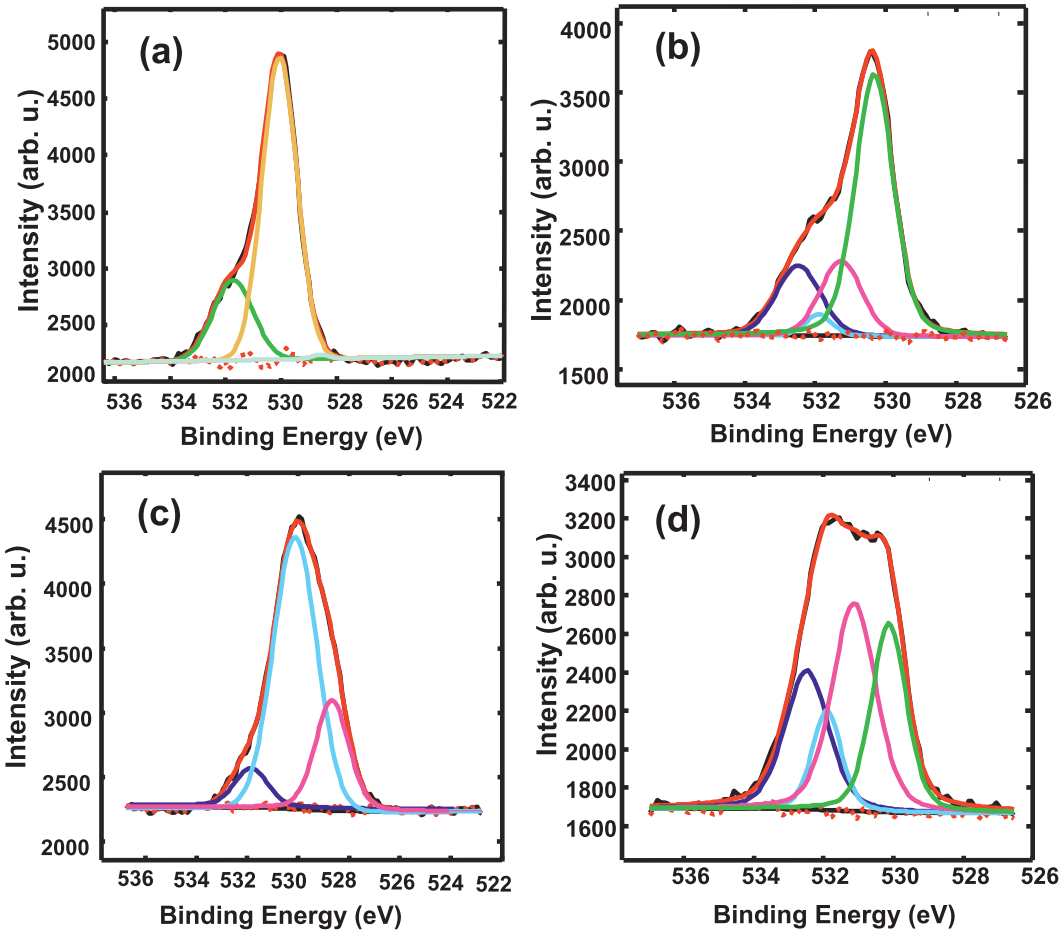

Fig. 12. XPS O1s spectra of (a and c) ZnO-4h@10.5pH and (b and d) ZnO-4h@12.5pH sensing layers before and after exposure to H_2S gas.

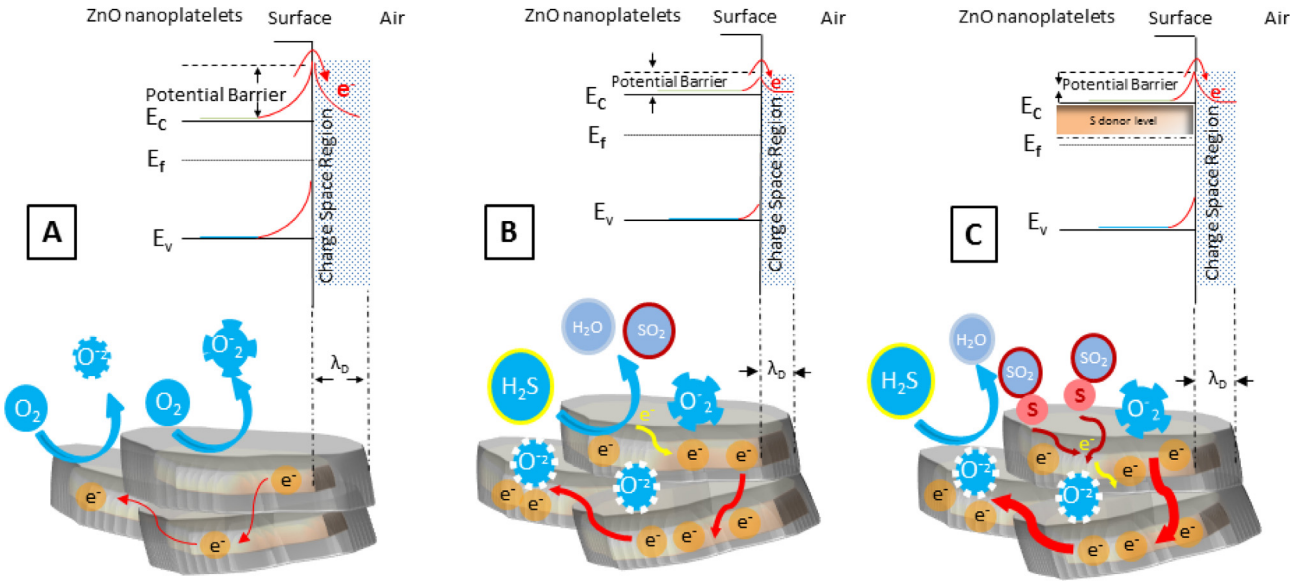

Scheme 2. Schematic diagram displaying the sensing mechanism of ZnO-4h@10.5pH towards H_2S at 75 °C.

Gas sensing mechanism based on ZnO nanoplatelets

The gas sensing mechanism of the fabricated ZnO metal-oxide semiconductor (MOS) can be governed by employing a surface-gas interaction model. It is well-known that for ZnO as an n-type MOS the conduction electrons are mostly created from point defects such as V_O (see reaction (1)), V_{Zn} (see reaction (2)) and Zn_i. A variation in a sensor resistance is mostly induced by the adsorption-desorption process of the gas molecules on the sensing material surface. The adsorption of oxygen species is strictly connected to the structural defects on the ZnO surface, particularly V_O, denoting that the more relative concentration of V_O, the more chemisorbed oxygen molecules on the surface of ZnO, which

can provide a plenty amount of active sites for gas molecules, to facilitate more gas molecules to be adsorbed on the sensing materials surface.

Therefore, the higher change in sensor resistance observed for the ZnO-4h@10.5pH in air can be justified by the higher relative concentration of V_O and higher S_{BET} and as well as paramagnetic defects as shown in Figs. 9 and S5a. We witnessed in Fig. 9 that the sensor response increased with an increase in point defects (which led to enhanced adsorption of oxygen molecules) and S_{BET}. This higher sensing behaviour linked with the surface defects and higher surface area is in good agreement with the observation reported by Li et al. [68] and Hosseini et al. [17] and that from our previous results [69].

Furthermore, by relating the sensing response with the paramagnetic defects we calculated the number of spins as presented in Fig. S5b. Remarkably, a clear constructive association between the electrical response and paramagnetic V_O is revealed, validating the PL and XPS findings. These observations are in line with the findings reported by D'Arienzo et al. [70] and Canevali et al. [71], who demonstrated that the quantity of the paramagnetic V_O identified by ESR is associated to that of the electrons reaching the conduction band of the SnO_2 and as a result matches the improvement in the sensing performance.

In Scheme 2A the atmospheric oxygen O_2 adsorbed from the surface of the ZnO nanoplatelets and consequently converted to ionized oxygen species, O_2^- and O^- at the operating temperature less than 150 °C. The adsorbed oxygen species then traps electrons from the ZnO nanoplatelets creating an increase in the electrical resistance, due to the formation of an electron-depletion layer on the nanoplatelets [56]. Therefore, these reactions (1)–(3), can be expressed using Kröger-Vink notation, where in this case V_O acts as electron donor and the surface relative concentration of V_O is governed by the interaction of surface oxidation by ambient oxygen molecules (depending on the reaction temperature, here 75 °C) and reduction by reducing gases (e.g. H_2S in this case).

$$Zno \rightarrow Zn_{Zn} + V_{\ddot{O}} + 1/2O_2 + 2e^- \quad (1)$$

$$V_{Zn}^X + V_O^X \Leftrightarrow null \quad (2)$$

$$O_O^X \rightarrow V_{\ddot{O}} + 1/2O_2 + e^- \quad (3)$$

When the ZnO nanoplatelets are exposed to H_2S (see Scheme 2B), it reacts with adsorbed oxygen species of the surface and causes a decrease of the electron-depletion layer and increases the conductivity of the material transferring electrons on it. The change in surface oxygen concentration is the main cause for the bending and the depletion layers which are explained the sensing mechanism under this condition. In Scheme 2C, we observe a drastic increase of the conductivity of the material, which corresponds to the formation of the shallow donor level from the decomposition of H_2S and the formation of Zn-S bonds in ZnO due to sulfuration mechanism. The chemisorbed S is being captured by the V_O of the intrinsic n-type ZnO causing a significant decrease of the height of the band bending. According to reactions (4) and (5) using the Kröger-Vink notation, H_2S interacts with lattice oxygen and produce V_O and SO_2 and as well as H_2O (see Scheme 2c), and this releases electrons to the conduction band after ionization [72].

$$H_2\,S + 2O_O^X \Leftrightarrow H_2\,O + V_{\ddot{O}} + SO_2 \quad (4)$$

$$H_2\,S + ZnO + O_O^X \rightarrow H_2\,O + ZnS + SO_2 + V_{\ddot{O}} \quad (5)$$

When the H_2S supply is stopped and introducing a dry air in the chamber, ZnS is converted back to ZnO, due to desulfurization reaction as shown in reaction (6):

$$ZnS + O_O^X \rightarrow ZnO + SO_2 \quad (6)$$

Conclusion and remarks

In summary, various ZnO nanostructures were synthesized and assessed as H_2S chemiresistive gas sensors. The sensor based on ZnO nanoplatelets prepared for 4 h at 10.5 pH exhibited enhanced gas-sensing performance and superior selectivity to H_2S, with insignificant cross-responses to interfering gases such as reducing gases (CH_4, CO and NH_3), VOCs (ethanol, acetone), some family of BTEX (benzene and toluene) and oxidizing gas (NO_2). The maximum response and sensitivity of approximately 450 and 14.04 ppm^{-1} were witnessed at an optimum operating temperature of 75 °C. This facilitated the capability to optimize the quality and specific morphology at controlled synthesis reaction time and pH. The superior response of the ZnO-4h@10.5pH based sensor is ascribed to higher relative concentration of the electron donors (V_O), allowing more dynamic oxygen molecules adsorption on the ZnO surface. The findings offered here established the prospective application of ZnO-4h@10.5pH based sensor for detection of H_2S gas.

Acknowledgements

This work was financially supported by the Department of Science and Technology and the Council for Scientific and Industrial Research, South Africa, Project numbers: HGER85X and HCDARD3). The authors wish to thank characterization facility at National Centre for Nano-Structured Materials – CSIR. IK wants to thank also Ms. Sharon Eggers and Ms. Charity Maepa for SEM analysis.

Appendix A. Supplementary data

Supplementary data to this article can be found online at https://doi.org/10.1016/j.rinp.2019.01.089.

References

[1] Srinivasan P, Jeyaprakash BG. Fabrication of highly selective formaldehyde sensor through a novel spray deposited ZnO/CdS heterostructured interface: A surface charge enhancement approach. J Alloy Compd 2018;768:1016–28.
[2] Kim T-H, Yoona J-W, Kang YC, Abdel-Hady F, Wazzan AA, Lee J-H. A strategy for ultrasensitive and selective detection of methylamine using p-type Cr_2O_3: morphological design of sensing materials, control of charge carrier concentrations, and configurational tuning of Au catalysts. Sens Actuators B 2017;240:1049–57.
[3] Kolhe Pankaj S, Shinde Alpana B, Kulkarni SG, Maiti N, Koinkar Pankaj M, Sonawane Kishor M. Gas sensing performance of Al doped ZnO thin film for H2S detection. J Alloys Compd 2018;748:6–11.
[4] Datta N, Ramgir N, Kaur M, Ganapathi SK, Debnath AK, Aswal DK, et al. Selective H_2S sensing characteristic of hydrothermally grown ZnO-nanowires network tailored by ultrathin CuO layers. Sens Actuators B 2012;166–167:394–401.
[5] Bhatia Sonik, Verma Neha, Bedi RK. Ethanol gas sensor based upon ZnO nanoparticles prepared by different techniques. Results Phys 2017;7:801–6.
[6] Janotti A, Van de Walle CG. Hydrogen multicentre bonds. Nat Mater 2007;6:44–7.
[7] Li GR, Hu T, Pan GL, Yan TY, Gao XP, Zhu HY. Morphology-function relationship of ZnO: polar planes, oxygen vacancies, and activity. J Phys Chem C 2008;112:11859–64.
[8] Korotcenkov G. The role of morphology and crystallographic structure of metal oxides in response of conductometric-type gas sensors. Mater Sci Eng R 2008;61:1–39.
[9] Fouad OA, Glaspell G, El-Shall MS. Structural, optical and gas sensing properties of ZnO, SnO_2 and ZTO nanostructures. NANO 2010;5:185–94.
[10] Pawar RC, Shaikh JS, Suryavanshi SS, Patil PS. Growth of ZnO nanodisk, nanospindles and nanoflowers for gas sensor: pH dependency. Curr Appl Phys 2012;12:778–83.
[11] Kim W, Choi M, Yong K. Generation of oxygen vacancies in ZnO nanorods/films and their effects on gas sensing properties. Sens Actuators B 2015;209:989–96.
[12] Wang Z, Xue J, Han D, Gu F. Controllable defect redistribution of ZnO nanopyramids with exposed 10–11 facets for enhanced gas sensing performance. ACS Appl Mater Interfaces 2015;7:308–17.
[13] Han N, Hu P, Zuo A, Zhang D, Tian Y, Chen Y. Photoluminescence investigation on the gas sensing property of ZnO nanorods prepared by plasma-enhanced CVD method. Sens Actuators B 2010;145:114–9.
[14] Zhang L, Zhao J, Lu H, Li L, Zheng J, Zhang J, et al. Highly sensitive and selective dimethylamine sensors based on hierarchical ZnO architectures composed of nanorods and nanosheet-assembled microspheres. Sens Actuators B 2012;171–172:1101–9.
[15] Tan ST, Tan CH, Chong WY, Yap CC, Umar AA, Ginting RT, et al. Microwave-assisted hydrolysis preparation of highly crystalline ZnO nanorod array for room

temperature photoluminescence-based CO gas sensor. Sens Actuators B 2016;22:304–12.
[16] Hosseini ZS, Iraji zad A, Mortezaali A. Room temperature H_2S gas sensor based on rather aligned ZnO nanorods with flower-like structures. Sens Actuators B 2015;207:865–71.
[17] Hosseini ZS, Mortezaali A, Zad AI, Fardindoost S. Sensitive and selective room temperature H_2S gas sensor based on Au sensitized vertical ZnO nanorods with flowerlike structures. J Alloys Compd 2015;628:222–9.
[18] Ghosh S, Adak D, Bhattacharyya R, Mukherjee N. ZnO/γ-Fe_2O_3 charge transfer interface toward highly selective H_2S sensing at a low operating temperature of 30 °C. ACS Sens 2017;2:1831–8.
[19] Ramgir NS, Sharma PK, Datta N, Kaur M, Debnath AK, Aswal DK, et al. Room temperature H_2S sensor based on Au modified ZnO nanowires. Sens Actuators B 2013;186:718–26.
[20] Qi G, Zhang L, Yuan Z. Improved H_2S gas sensing properties of ZnO nanorods decorated by a several nm ZnS thin layer. Phys Chem Chem Phys 2014;16:13434–9.
[21] Mani GK, Rayappan JBB. Facile synthesis of ZnO nanostructures by spray pyrolysis technique and its application as highly selective H_2S sensor. Mater Lett 2015;158:373–6.
[22] Motaung DE, Mhlongo GH, Bolokang AS, Dhonge BP, Swart HC, Ray SS. Improved sensitivity and selectivity of pristine zinc oxide nanostructures to H_2S gas: detailed study on the synthesis reaction time. Appl Surf Sci 2016;386:210–23.
[23] Oosthuizen DN, Motaung DE, Swart HC. In depth study on the notable room-temperature NO_2 gas sensor based on CuO nanoplatelets prepared by sonochemical method: Comparison of various bases. Sens Actuators B 2018;266:761–72.
[24] Patterson AL. The Scherrer formula for x-ray particle size determination. Phys Rev 1939;56:978–82.
[25] Pal U, Santiago P. Controlling the morphology of ZnO nanostructures in a low-temperature hydrothermal process. J Phys Chem B 2005;109:15317–21.
[26] Ghoderao KP, Jamble SN, Kale RB. Influence of pH on hydrothermally derived ZnO nanostructures. Optik 2018;156:758–71.
[27] Tshabalala ZP, Motaung DE, Mhlongo GH, Ntwaeaborwa OM. Facile synthesis of improved room temperature gas sensing properties of TiO_2 nanostructures: effect of acid treatment. Sens Actuators B 2016;224:841–56.
[28] Wang J, Chen R, Xiang L, Komarneni S. Synthesis, properties and applications of ZnO nanomaterials with oxygen vacancies: a review. Ceram Int 2018;44:7357–77.
[29] Lupan O, Ursaki VV, Chai G, Chow L, Emelchenko GA, Tiginyanu IM, et al. Selective hydrogen gas nanosensor using individual ZnO nanowire with fast response at room temperature. Sens Actuators B 2010;144:56–66.
[30] Djurišić AB, Leung YH, Tam KH, Hsu YF, Ding L, Ge WK, et al. Defect emissions in ZnO nanostructures. Nanotechnology 2007;18:095702–11.
[31] Lin CY, Wang WH, Lee C-S, Sun KW, Suen YW. Magneto photoluminescence properties of Co-doped ZnO nanorods. Appl Phys Lett 2009;94:151909–1519011.
[32] Wang YG, Lau SP, Zhang XH, Hng HH, Lee HW, Yu SF, et al. Enhancement of near-band-edge photoluminescence from ZnO films by face-to-face annealing. J Cryst Growth 2003;259:335–42.
[33] Janotti A, Van de Walle CG. Native point defects in ZnO. Phys Rev B 2007;76:165202–23.
[34] Reynolds DC, Look DC, Jogai B, Van Nostrand JE, Jones R, Jenny J. Source of the yellow luminescence band in GaN grown by gas-source molecular beam epitaxy and the green luminescence band in single crystal ZnO. Solid State Commun 1998;106:701–4.
[35] Cross RBM, De Souza MM, Narayanan EMS. A low temperature combination method for the production of ZnO nanowires. Nanotechnology 2005;16:2188–92.
[36] Gomi M, Oohira N, Ozaki K, Koyano M. Photoluminescent and structural properties of precipitated ZnO fine particles. Jpn J Appl Phys 2003;42:481–5.
[37] Schneider JJ, Hoffmann RC, Engstler J, Klyszcz A, Erdem E, Jakes P, et al. Synthesis, characterization, defect chemistry, and FET properties of microwave-derived nanoscaled zinc oxide. Chem Mater 2010;22:2203–12.
[38] Repp S, Erdem E. Controlling the exciton energy of zinc oxide (ZnO) quantum dots by changing the confinement conditions. Spectrochim Acta Part A 2016;152:637–44.
[39] Dhakshinamoorthy J, Pullithadathil B. New insights towards electron transport mechanism of highly efficient p-type CuO (111) nanocuboids-based H_2S gas sensor. J Phys Chem C 2016;120:4087–96.
[40] Wang C, Chu X, Wu M. Detection of H_2S down to ppb levels at room temperature using sensors based on ZnO nanorods. Sens Actuators B 2006;113:320–3.
[41] Liu Z, Fan T, Zhang D, Gong X, Xu J. Hierarchically porous ZnO with sensitivity and selectivity to H_2S derived from biotemplates. Sens Actuators B 2009;136:499–509.
[42] Diao K, Zhou M, Zhang J, Tang Y, Wang S, Cui X. High response to H_2S gas with facile synthesized hierarchical ZnO microstructures. Sens Actuators B 2015;219:30–7.
[43] Rout CS, Hegde M, Govindaraj A, Rao CNR. Ammonia sensors based on metal oxide nanostructures. Nanotechnology 2007;18:205504–13.
[44] Chen YJ, Zhu CL, Xiao G. Reduced-temperature ethanol sensing characteristics of flower-like ZnO nanorods synthesized by a sonochemical method. Nanotechnology 2006;17:4537–41.
[45] Calestani D, Zha M, Mosca R, Zappettini A, Carotta MC, Natale VD, et al. Growth of ZnO tetrapods for nanostructure-based gas sensors. Sens Actuators B 2010;144:472–8.
[46] Xu J, Wang X, Shen J. Hydrothermal synthesis of In_2O_3 for detecting H_2S in air. Sens Actuators B 2006;115:642–6.
[47] Na CW, Park S-Y, Chung J-H, Lee J-H. Transformation of ZnO nanobelts into single-crystalline Mn_3O_4 nanowires. ACS Appl Mater Interfaces 2012;4:6565–72.
[48] Jo Y-M, Kim T-H, Lee C-S, Lim K, Na CW, Abdel-Hady F, et al. Metal-organic framework-derived hollow hierarchical Co_3O_4 nanocages with tunable size and morphology: ultrasensitive and highly selective detection of methylbenzenes. ACS Appl Mater Interfaces 2018;10:8860–8.
[49] Kaur M, Ganapathi K, Mukund V, Jain C, Ramgir NS, Datta N, et al. Mater. Lett. 2014;143:1319–24.
[50] Deng J, Fu Q, Luo W, Tong X, Xiong J, Hu Y, Zheng Z. Enhanced H2S gas sensing properties of undoped ZnO nanocrystalline films from QDs by low-temperature processing. Sens Actuators B 2016;224:153–8.
[51] Guo Y, Gong M, Li Y, Liu Y, Dou X. Sensitive, selective, and fast detection of ppb-level H_2S gas boosted by ZnO-CuO mesocrystal. Nanoscale Res Lett 2016;11:475–84.
[52] Meng F, Zhao G, Zhang H. Solvothermal synthesis and H_2S gas sensing characteristics of ZnO nanorods. Nanosci Nanotechnol Lett 2013;5:1012–8.
[53] Huang H, Xu P, Zheng D, Chen C, Li X. J Mater Chem A 2015;3:6330–9.
[54] Katoch A, Choi S-W, Kim J-H, Lee JH, Lee J-S, Kim SS. Importance of the nanograin size on the H_2S-sensing properties of ZnO–CuO composite nanofibers. Sens Actuators B 2015;214:111–6.
[55] Cao Y, Jia D, Wang R, Lu J. o Rapid one-step room-temperature solid-state synthesis and formation mechanism of ZnO nanorods as H_2S-sensing materials. Solid-State Electron 2013;82:67–71.
[56] Shewale PS, Yu YS. H_2S gas sensing properties of undoped and Ti doped ZnO thin films deposited by chemical spray pyrolysis. J Alloys Compd 2016;684:428–37.
[57] Shewale PS, Patil VB, Shin SW, Kim JH, Uplane MD. H_2S gas sensing properties of nanocrystalline Cu-doped ZnO thin films prepared by advanced spray pyrolysis. Sens Actuators B 2013;186:226–34.
[58] Woo H-S, Kwak C-H, Kim I-D, Lee J-H. Selective, sensitive, and reversible detection of H_2S using Mo-doped ZnO nanowire network sensors. J Mater Chem A 2014;2:6412–8.
[59] Hieu NM, Kim H, Kim C, Hong S-K, Kim D. A hydrogen sulfide gas sensor based on Pd-decorated ZnO nanorods. J Nanosci Nanotechnol 2016;16:10351–5.
[60] Ghimbeu CM, Schoonman J, Lumbreras M, Siadat M. Electrostatic spray deposited zinc oxide films for gas sensor applications. Appl Surf Sci 2007;253:7483–9.
[61] Kim J, Yong K. Mechanism study of ZnO nanorod-bundle sensors for H_2S gas sensing. J Phys Chem C 2011;115:7218–24.
[62] Qin Y, Zhang X, Wang Y, Liu Y. Remarkable improvement of $W_{18}O_{49}/TiO_2$ heteronanowires in ambient temperature-responsive NO_2-sensing abilities and its unexpected n-p transition phenomenon. Sens Actuators B 2017;240:477–86.
[63] Nasrabadi MN, Mortazavi Y, Khodadadi AA. Highly sensitive and selectiveGd_2O_3-doped SnO_2 ethanol sensors synthesized by a high temperature and pressure solvothermal method in a microreactor. Sens Actuators B 2016;230:130–9.
[64] Ponnuvelu DV, Abdulla S, Pullithadathil B. Highly monodispersed mesoporous, heterojunction ZnO@Au microspheres for trace-level detection of NO_2 gas. Microporous Mesoporous Mater 2018;255:156–65.
[65] Pavelko RG, Vasiliev AA, Llobet E, Sevastyanov VG, Kuznetsov NT. Selectivity problem of SnO_2 based materials in the presence of water vapors. Sens Actuators B 2012;170:51–9.
[66] Viter R, Iatsunskyi I, Fedorenko V, Tumenas S, Balevicius Z, Ramanavicius A, et al. Enhancement of electronic and optical properties of ZnO/Al_2O_3 nanolaminate coated electrospun nanofibers. J Phys Chem C 2016;120:5124–32.
[67] Lu SW, Schmidt HK. Photoluminescence and XPS analyses of Mn^{2+} doped ZnS nanocrystals embedded in sol–gel derived hybrid coatings. Mater Res Bull 2008;43:583–9.
[68] Li D, Qin L, Zhao P, Zhang Y, Liu D, Liu F, et al. Preparation and gas-sensing performances of ZnO/CuO rough nanotubular arrays for low-working temperature H_2S detection. Sens Actuators B 2018;254:834–41.
[69] Kortidis I, Swart HC, Ray SS, Motaung DE. Characteristics of point defects on the room temperature ferromagnetic and highly NO_2 selectivity gas sensing of p-type Mn_3O_4 nanorods. Sens Actuators B 2019;285:92–107.
[70] D'Arienzo M, Cristofori D, Scotti R, Morazzoni F. New insights into the SnO_2 sensing mechanism based on the properties of shape controlled tin oxide nanoparticles. Chem Mater 2013;25:3675–86.
[71] Canevali C, Mari CM, Mattoni M, Morazzoni F, Nodari L, Russo U, et al. Phys Chem B 2005;109:7195–202.
[72] Li S-M, Zhang L-X, Zhu M-Y, Ji G-J, Zhao L-X, Yinc J, et al. Acetone sensing of ZnO nanosheets synthesized using room-temperature precipitation. Sens Actuators B 2017;249:611–23.